Locomotor Adaptation Is Associated with Microstructural Properties of the Inferior Cerebellar Peduncle

Sivan Jossinger[1] • Firas Mawase[2] • Michal Ben-Shachar[1,3] • Lior Shmuelof[4,5,6]

Abstract

In sensorimotor adaptation paradigms, participants learn to adjust their behavior in response to an external perturbation. Locomotor adaptation and reaching adaptation depend on the cerebellum and are accompanied by changes in functional connectivity in cortico-cerebellar circuits. In order to gain a better understanding of the particular cerebellar projections involved in locomotor adaptation, we assessed the contribution of specific white matter pathways to the magnitude of locomotor adaptation and to long-term motor adaptation effects (recall and relearning). Diffusion magnetic resonance imaging with deterministic tractography was used to delineate the inferior and superior cerebellar peduncles (ICP, SCP) and the corticospinal tract (CST). Correlations were calculated to assess the association between the diffusivity values along the tracts and behavioral measures of locomotor adaptation. The results point to a significant correlation between the magnitude of adaptation and diffusivity values in the left ICP. Specifically, a higher magnitude of adaptation was associated with higher mean diffusivity and with lower anisotropy values in the left ICP, but not in other pathways. Post hoc analysis revealed that the effect stems from radial, not axial, diffusivity. The magnitude of adaptation was further associated with the degree of ICP lateralization, such that greater adaptation magnitude was correlated with increased rightward asymmetry of the ICP. Our findings suggest that the magnitude of locomotor adaptation depends on afferent signals to the cerebellum, transmitted via the ICP, and point to the contribution of error detection to locomotor adaptation rate.

Michal Ben-Shachar and Lior Shmuelof contributed equally to this work.

✉ Sivan Jossinger
   sivanyoss@gmail.com

1   The Gonda Multidisciplinary Brain Research Center, Bar-Ilan University, Ramat-Gan, Israel

2   Faculty of Biomedical Engineering, Technion–Israel Institute of Technology, Haifa, Israel

3   The Department of English Literature and Linguistics, Bar-Ilan University, Ramat-Gan, Israel

4   Zlotowski Center for Neuroscience, Ben-Gurion University of the Negev, Beer-Sheva, Israel

5   Department of Brain and Cognitive Sciences, Ben-Gurion University of the Negev, Beer-Sheva, Israel

6   Department of Physiology and Cell Biology, Ben-Gurion University of the Negev, Beer-Sheva, Israel

Introduction

Motor adaptation is the process by which subjects learn to adjust their movements to changes in environmental demands. Theoretical frameworks suggest that adaptation is achieved by updating internal models of the environmental dynamics based on sensory prediction errors (see [1] for review). For example, when subjects are introduced to a split-belt treadmill, where one leg is forced to move faster than the other, they gradually learn to adjust their stance and swing times in order to overcome the external perturbation and improve their dynamic balance. Then, if the perturbation is unexpectedly removed, subjects will typically show aftereffects—a mirror image of the previously learned gait cycle [2], indicating the adjustment of their internal model to the perturbation [1, 3, 4]. Adaptation underlies the successful interaction between the nervous system and changes in the environment [5]. Here, we examine the neural pathways that are associated with locomotor adaptation.

Converging experimental evidence points to the cerebellum as a key structure in the process of motor adaptation. Patients with cerebellar lesions present an impaired ability to adapt their movements during motor adaptation tasks such as visuomotor adaptation [6, 7], adaptation to a force field [8], and locomotor adaptation [9]. By using transcranial direct current stimulation (tDCS) in healthy adults, it has been shown that a temporary change in the activity of the cerebellum significantly influences the adaptation of reaching movements [10, 11]. Neuroimaging studies have found a significant increase in cerebellar activity not only at the beginning of the adaptation phase [12, 13] but also after learning has been acquired [14], as well as when subjects are asked to recall the previously learned motor skill [15]. Despite the converging results regarding the involvement of the cerebellum in adaptation, the interactions between the cerebellum and the cortical and subcortical motor systems have yet to be fully elucidated. In the current study, we examine the anatomical connections of the cerebellum with extra-cerebellar brain regions and assess their unique contribution to different components of motor adaptation.

Adaptation can be seen in multiple behaviors, including walking. Locomotor adaptation is essential for maintaining balance when walking in different terrains, speeds, and trajectories. This type of adaptation can be tested with the split-belt treadmill. During the split-belt walking test, participants learn to adapt to the split-belt perturbation by changing the duration of their left and right strides and regaining symmetry between their lengths [2, 16]. In addition to the short-term process of adaptation, split-belt walking is also accompanied by long-term behavioral changes manifested in measures of recall—the retrieval of a previous successful action, and relearning—an increased sensitivity to errors when the same perturbation is introduced again [10, 15, 17].

The magnitude of adaptation to the split-belt manipulation has been shown to depend on cerebellar activity [18], which has been repeatedly shown to encode movement errors [19–21]. These "error detection" signals, originating in the inferior olivary neurons, are carried to the cerebellar cortex by the climbing fibers. Hence, the olivo-cerebellar connections may have a central role in the initial phase of adaptation, where adequate error detection is crucial. In contrast, long-term components of locomotor adaptation were previously associated with cerebro-cerebellar loops. Specifically, by measuring resting-state fMRI before and after exposure to the split-belt manipulation, Mawase et al. [17] showed that recall is correlated with baseline thalamocortical connectivity, whereas relearning is correlated with baseline cerebellar-thalamic connectivity.

Connectivity between the cerebellum and other parts of the nervous system is based solely on three white matter pathways: the inferior cerebellar peduncle (ICP), middle cerebellar peduncle (MCP), and superior cerebellar peduncle (SCP) [22].

The ICP is mainly composed of cerebellar afferent fibers feeding signals from the spine and the olivary nucleus into the cerebellum. The ICP also conveys efferent signals from the cerebellum towards the vestibular nuclei. The MCP is mainly composed of afferent fibers carrying input information from the cerebral cortex via the pontine nuclei to the contralateral cerebellar cortex. Finally, the SCP is mainly composed of efferent fibers that carry information from the deep cerebellar nuclei to the contralateral cortex via the thalamus, decussating at the level of the inferior colliculi [22].

In the current study, we adopted a hypothesis-driven approach, focusing on three specific tracts that are suspected to mediate locomotor adaptation. We tested the hypothesis that locomotor adaptation, which is an error-driven process, is associated with microstructural properties of the ICP, connecting the inferior olive and the cerebellum. This hypothesis is based on the widely accepted view that complex spikes discharge, emerging from the inferior olive, encode errors in motor performance [19]. We further hypothesized that recall is associated with the corticospinal tract (CST), transmitting signals from the motor cortex to the skeletal muscles via the thalamus [23] and that relearning is associated with the SCP connecting the cerebellum and the thalamus. These latter two hypotheses are based on functional connectivity findings associating long-term components of locomotor adaptation with changes in the functional connectivity of cortico-cerebellar circuits [17]. To test our hypotheses, we introduced subjects with the split-belt treadmill task, which enabled us to estimate their performance during adaptation, recall, and relearning. We used diffusion magnetic resonance imaging (dMRI) and tractography to delineate the ICP, CST, and SCP in each individual's native space. We then analyzed the relations between diffusivity parameters extracted from each tract and the corresponding behavioral measure. We thus used static, structural properties of specific white matter tracts to predict dynamic, functional changes that accompany locomotor adaptation. By using this approach, we aim to pinpoint the role of specific white matter pathways in locomotor adaptation and to extend the current knowledge regarding the neuroanatomical basis of this error-driven learning procedure.

Methods

Participants

Seventeen healthy adults (eight females and nine males; mean age 27.94, age range 23–40 years) were recruited as part of a multimodal MRI study on locomotor adaptation. Functional MRI results from this study have already been published [17]. However, this is the first analysis of diffusion MRI data collected as part of this study (data collected in 2014). The participants did not have a history of neurological diseases and/or

psychological disorders. This study was approved by the Helsinki committee of Soroka Medical Center, Beer-Sheva, Israel. All participants were naïve to the purpose of the study and had no prior experience with the behavioral paradigm.

Behavioral Procedure

A split-belt treadmill paradigm was used to assess locomotor adaptation (Fig. 1). The split-belt treadmill (ForceLink, Clemborg, The Netherlands) consists of two independent belts, one under each leg, which can be set independently to move at the same speed or at different speeds. In this study, participants took part in three treadmill sessions on three consecutive days (Fig. 1a). On the first day, participants underwent 20 min of baseline walking, in which the two belts moved at the same speed (0.7 m/s). On the second day, participants were exposed to a split-belt condition for 20 min, in which each belt was set to move at a different speed, forcing the participants to adjust their steps to the imposed perturbation. For all participants, the non-dominant leg was forced to move two times faster than the dominant leg (1.4 m/s vs. 0.7 m/s), as previously done in cerebellar patient studies [9]. To determine leg dominance, we instructed the participants to kick a ball 3 times and to report their leg selection. This task was chosen based on previous results showing that daily tasks, such as kicking a ball, show stable foot preference [24].

On the third day, participants performed three consecutive blocks of treadmill walking: the first block consisted of split-belt walking for 10 min, assessing recall of the learned pattern. In the second block, participants returned to baseline walking for 10 min, washing out the previously adapted walking pattern. Finally, the third block consisted of another 20-min session of split-belt walking, in order to assess relearning. The

specific parameters chosen here (e.g., time intervals between the blocks, etc.) have effectively produced significant recall and relearning effects in this dataset, as shown before [17].

Quantifying Components of Locomotor Adaptation

Motor adaptation can be thought of as an error-driven learning process in which the agent is directed to minimize motor errors [25]. Hence, the relevant measure of learning in motor adaptation paradigms is the change in motor errors throughout the task. It has been previously proposed that locomotor adaptation is driven by kinematic errors, which are reflected in the asymmetry of the left and right step-length [2]. During walking on the split-belt treadmill, participants learn to adapt to the perturbation by minimizing the asymmetry between their steps [2, 16, 17]. Here, in order to quantify the short- and long-term components of locomotor adaptation, we first measured step asymmetry in each bipedal gait cycle (Fig. 1b). Then, we summarized the measure of step asymmetry at three key points along each day of the task to evaluate the motor errors at the initial, middle, and late phase of the adaptation. Finally, by using the summarized errors, we calculated three behavioral components of locomotor adaptation: (1) adaptation magnitude—representing a short-term process of error reduction; (2) recall—refers to the retrieval of previous motor patterns from memory; (3) relearning—describes the performance when participants are re-exposed to the same perturbation after a washout period (Fig. 1b).

Step asymmetry was defined as the normalized difference between the length of the left and right steps in each bipedal cycle. To calculate the length of each step, we recorded the dynamics of the walking behavior by using force sensors that were embedded in the treadmill (sampled at 500 Hz). The
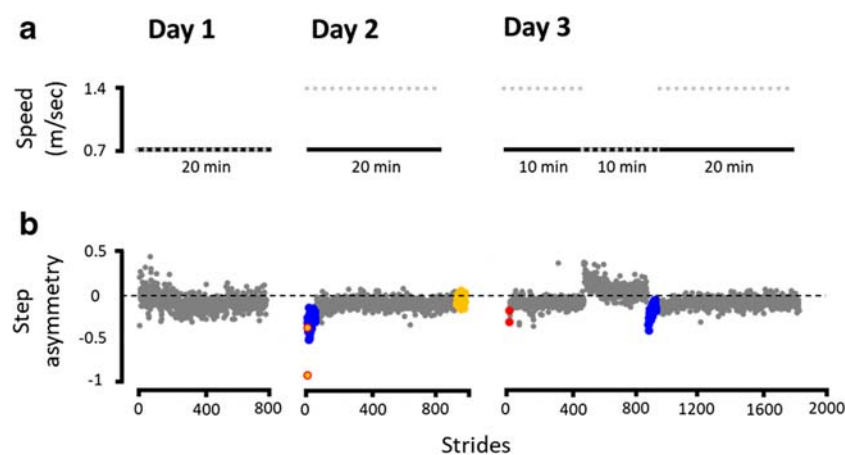
Fig. 1 The split-belt task. **a** Experimental design. Subjects participated in three split-belt walking sessions over three consecutive days. Solid black line indicates the right leg. Gray-dashed line indicates the left leg. See text for details. **b** Definition of behavioral measures. Shown is the performance of a representative subject on the split-belt treadmill task. Gray circles represent the participant's step asymmetry in each stride.

Adaptation magnitude on day 2 was calculated as the difference in step asymmetry between initial errors (yellow circles with red contour) and late errors (yellow). Recall was defined as the difference between the initial errors on day 2 (yellow circles with red contour) and day 3 (full red circles). Relearning was defined as the difference between mid-errors in day 3 and mid-errors on day 2 (blue)

length of each step was measured as the distance between the point where one foot touched the belt, to the point where the toe of the opposing foot lifted off the belt. The left step length, for example, was measured as the distance between the initial contact of the left leg with the belt, to the point where the toe of the right foot lifted off the belt. Hence, our measure of step asymmetry was calculated as follows:

$$Step\ asymmetry = \frac{left\ step\ length - right\ step\ length}{left\ step\ length + right\ step\ length}$$

Motor errors were quantified as the size of step asymmetry: when the value of step asymmetry was zero, it indicated no motor errors, and as this value grew larger (in absolute value), it indicated larger motor errors. Motor errors were further summarized at three points along each split-belt session at each day of the experiment (Fig. 1b): initial errors were quantified as the mean step asymmetry at the first two strides; mid-errors were quantified as the mean step asymmetry at strides 3–50; asymptotic performance was calculated as the mean step asymmetry at the last 50 strides. These data epochs were selected to be consistent with [17] and similar to previous studies investigating locomotor adaptation with the split-belt treadmill paradigm in humans [26, 27].

The short- and long-term behavioral components of locomotor adaptation were calculated based on the initial errors, mid-errors, and asymptotic performance (Fig. 1b). *Adaptation magnitude* was defined as the difference between the initial error in day 2 (yellow circles with the red contour in Fig. 1b) and the asymptotic performance in day 2 (yellow), representing the reduction in motor errors throughout the second day of the experiment. *Recall* was calculated as the difference between the initial errors on day 3 (full red circles) and the initial errors on day 2 (yellow circles with red contour), representing how well participants remember the previously acquired motor pattern. *Relearning* was estimated as the signed difference between the mid-errors during re-adaptation of day 3 (blue) and mid-errors during adaptation of day 2 (blue), representing how fast the participants can re-learn the task after a short wash-out session [17].

MRI Data Acquisition

MRI scans were performed on a 3T Philips Achieva MRI scanner at the Soroka Medical Center. The MRI protocol included standard anatomical and diffusion imaging sequences, as detailed below. Functional MRI scans were also included in the scan protocol but are not reported here (see [17]). The structural MRI scans (i.e., T1 images and diffusion-weighted images) were acquired on the first day of the experiment (i.e., day 1), immediately after the baseline walking session. These baseline diffusivity measures of the white matter tracts were

then used to predict specific aspects of locomotor adaptation that take place on day 2 and day 3.

T1 Image Acquisition

High-resolution T1 anatomical images were acquired using a 3D fast spoiled gradient-echo (FSPGR) sequence, with a spatial resolution of $1 \times 1 \times 1$ mm (TR = 8165 ms, TE = 3.74 ms, 256×256 acquisition matrix), covering the entire cerebrum and cerebellum.

Diffusion-Weighted Image Acquisition

A standard diffusion MRI (dMRI) protocol was applied by means of a single-shot spin-echo diffusion-weighted echo-planar imaging (DW-EPI) sequence (60 axial slices, 2 mm thick, with a 0.2 mm gap; matrix size = 128×128, with a voxel size of $1.75 \times 1.75 \times 2$ cubic mm). dMRI data were acquired along 32 non-collinear gradient directions ($b = 800$ s/mm^2) and one reference volume ($b = 0$ s/mm^2). During the dMRI scan, participants were asked to lie still, and their head motion was minimized by placing cushions around their heads.

Imaging Data Analysis

Software

Data analysis was conducted using Matlab 2012b (The Mathworks, Natick, MA). For data preprocessing, the open-sourced 'mrDiffusion' package was used (https://github.com/vistalab/vistasoft/tree/master/mrDiffusion). Tract identification and quantification were implemented with the AFQ toolkit [28].

Data Preprocessing

Diffusion MRI data were preprocessed in native space for each individual separately, following a published pipeline [29–31]. This pipeline included a rigid transformation of the volume anatomy to the anterior commissure-posterior commissure (AC-PC) orientation, motion- and eddy-current correction of the diffusion-weighted echo-planar imaging (DW-EPI) data, alignment of DW-EPI data to the volume anatomy with the corresponding recalculation of the diffusion directions, resampling and tensor fitting. T1 images were rotated to the AC-PC plane following manual identification of the anterior and posterior commissures. Diffusion-weighted images were corrected for eddy-current and head motion distortions by using a 14-parameter constrained non-linear co-registration algorithm based on the expected pattern of eddy-current distortions [32]. Additionally, diffusion data were aligned to the anatomical volume by registering the b0 images to the T1 image using a rigid body mutual-information

maximization algorithm (as implemented in SPM5 [33]). The combined transform, resulting from both eddy-current correction and anatomical alignment, was applied to the raw diffusion data, and the diffusion data were resampled at $2 \times 2 \times 2$ cubic mm isotropic voxels. Gradient directions were adjusted according to the same transformation [34].

Diffusion tensors were fit to the registered diffusion data using a least-squares algorithm. Then, using tensor decomposition, we extracted the three eigenvectors and eigenvalues of the tensor, and in each voxel calculated fractional anisotropy (FA), mean diffusivity (MD), axial diffusivity (AD), and radial diffusivity (RD). FA was calculated as the normalized standard deviation of the eigenvalues. MD was calculated as the average of the three eigenvalues. AD was defined as the eigenvalue of the first eigenvector (diffusivity along the principal eigenvector). RD was defined as the average diffusivity of the second and third eigenvalues.

Tract Identification and Segmentation

In each individual's native space, we identified three white matter pathways involved in the transmission of signals relevant for locomotor adaptation: (1) the left ICP, connecting the spine and the olivary nucleus with the left cerebellar cortex; (2) the left SCP, connecting the left cerebellar nuclei and the right thalamus; (3) the right CST, connecting the right thalamus with the right primary motor cortex (Fig. 2a–c). We limited our tracts of interest within the cerebellar-thalamic-cortical loop to those which are associated with the left leg. This decision is based on previous findings showing that the change in step length throughout the adaptation is more

profound for the leg that moved on the faster belt (for example: see [35] Fig. 7A, [36] Fig. 5D). Moreover, it was previously shown that locomotor adaptation modulates the resting-state functional connectivity of the cerebellar-thalamic-cortical loop associated with the fast leg [17]. To identify these tracts and quantify their diffusion parameters, we used the AFQ package [28], implemented in Matlab (The Mathworks, Natick, MA), which consists of the following steps: (1) whole-brain fiber tractography, (2) region-of-interest (ROI)-based tract segmentation and cleaning, (3) quantification of diffusion parameters along the tract.

A whole-brain fiber group was tracked using a deterministic streamline tractography (STT) algorithm [37, 38] with a fourth-order Runge–Kutta path integration method and 1-mm fixed step size. To segment the tracts, we used a multiple-ROI approach in which the whole-brain fiber group was intersected with predefined ROIs using logical operations. The ROIs were first defined on a T1 template, and then back-transformed to each participant's native space (see [39] Fig. 3, for the position of the ROIs of the left ICP and the left SCP; see [40], Fig. 4, for the position of the ROIs of the right CST). After tract segmentation, an automated cleaning procedure was applied to remove outlier streamlines from each individual's tract. For the cerebellar peduncles, fibers were removed if they were longer than 1 standard deviation from the mean fiber length and spatially deviated more than 4 standard deviations from the core of the tract [39]. For the CST, fibers were removed if they were longer than 4 standard deviations from the mean fiber length and spatially deviated more than 5 standard deviations from the core of the tract [28]. Finally, diffusion properties were calculated at equidistant nodes along the tract (30
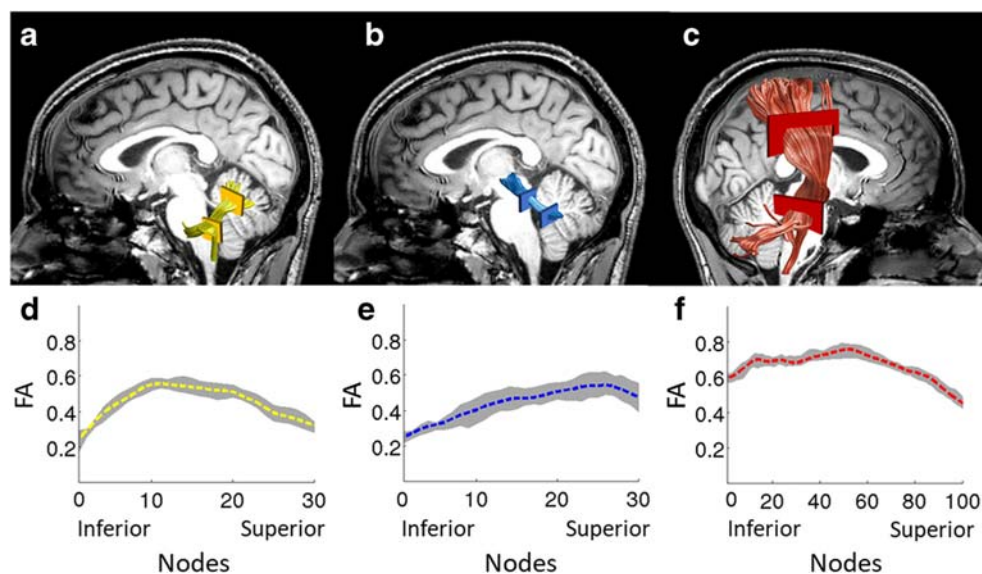

Fig. 2 Tracts of interest. a–c Tracts of interest identified in a single subject. The left ICP (a; yellow), left SCP (b; blue), and right CST (c; red) are visualized with their corresponding ROIs. The tracts are overlaid on a T1 sagittal image. d–f FA tract profiles of the left ICP (d; yellow), the left SCP (e; blue), and the right CST (f; red). Group-averaged FA profiles are plotted for equidistant locations between two defining ROIs, from the inferior ROI to the superior ROI. Boundaries of the 25th and 75th percentiles are indicated by gray shading
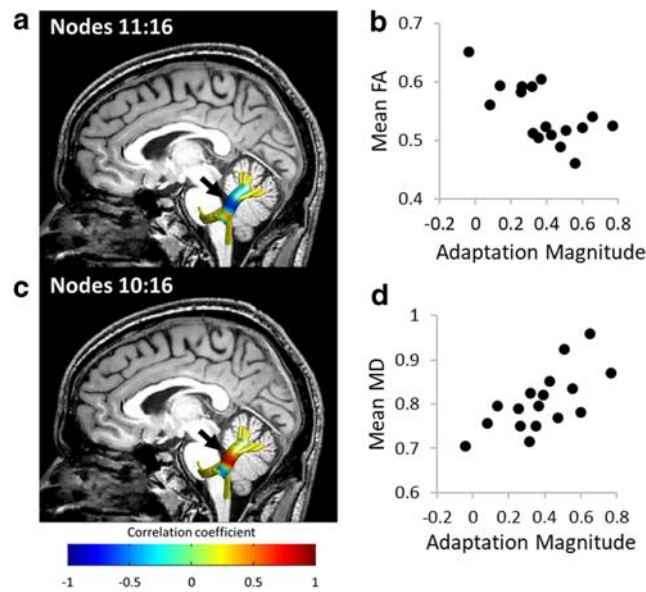
Fig. 3 Adaptation magnitude is correlated with white matter microstructure in the ICP. **a** The left ICP is shown in a single participant, overlaid on a midsagittal T1 image of the same individual. Colored overlay represents Spearman's *r* values between adaptation magnitude and FA in each node along the core of the tract. The black arrow points to the significant cluster ($p < 0.05$, FWE corrected). The color bar for panels **a** and **c** appears below panel **c**. **b** For each participant, the mean FA value of the significant cluster in panel **a** is plotted against the adaptation magnitude of the same individual ($r^2 = 0.34$). **c**, **d** Same as in **a** and **b**, respectively, but for MD values ($r^2 = 0.48$)
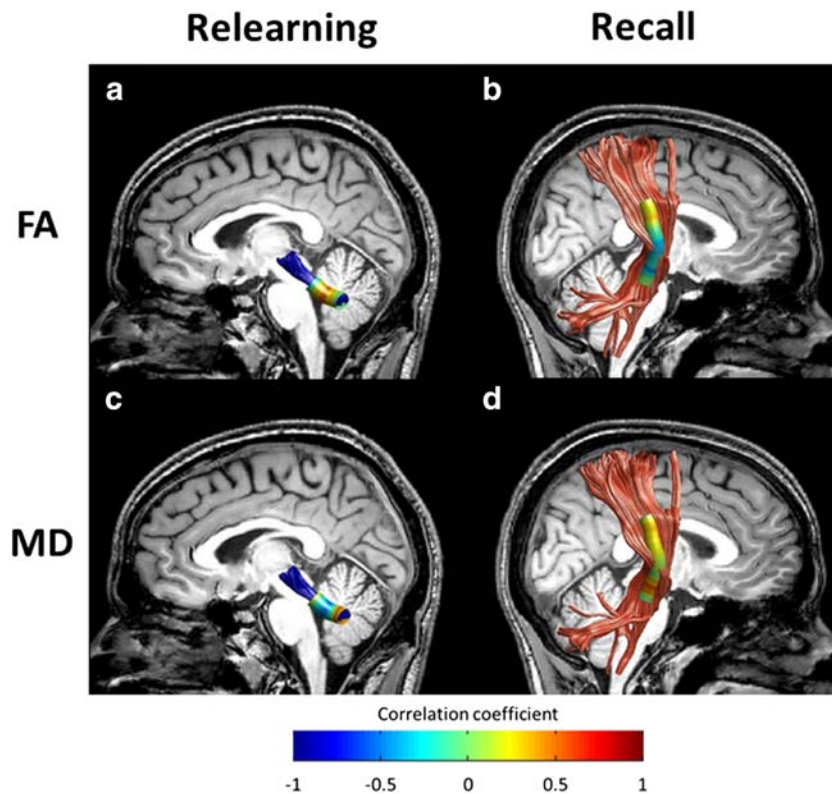
Fig. 4 Non-significant correlations in the SCP and CST. **a** The left SCP is shown in a single participant, overlaid on a midsagittal T1 image of the same individual. Colored overlay represents Spearman's *r* values between relearning and FA in each node along the core of the tract. **b** The right CST is shown in a single participant, overlaid on a midsagittal T1 image of the same individual. Colored overlay represents Spearman's *r* values between recall and FA in each node along the core of the tract. **c**, **d** Same as in **a** and **b**, respectively, but for MD values

nodes for the shorter cerebellar peduncles, and 100 nodes for the CST; [28, 39]) (Fig. 2d–f; S1).

Statistical Analysis

Brain-Behavior Correlations

Spearman's rank-order correlations were calculated to assess the associations between an individual's diffusion data and locomotor adaptation. Specifically, we used correlation analyses to test the link between (1) the left ICP and adaptation magnitude, (2) the left SCP and relearning, and (3) the right CST and recall (see Introduction for the motivation and hypotheses guiding these analyses). Neurocognitive correlations were calculated using two different approaches. First, we calculated the average diffusivity (FA or MD) of the core of the white matter tract and assessed the correlation between the mean tract diffusivity and its corresponding behavioral measure. Second, to gain further sensitivity, we assessed the correlations between behavioral measures and local diffusivity parameters at different points along the tract (see [28] for detailed motivation and methods). To this end, we divided the tracts to equidistant nodes placed along the central portion of the tract. Both analyses were restricted to the core of the tracts, enclosed between the two ROIs, and excluding tract endings, because the extreme segments of the tracts are extremely variable across individuals.

We assessed the correlation between the diffusivity values and corresponding behavioral measures in each of the nodes. Significance was corrected for multiple comparisons using a nonparametric permutation method, yielding a family-wise error (FWE) corrected alpha value of 0.05 [41]. To be considered a significant cluster of nodes, the cluster should satisfy two criteria: (1) each node in the cluster correlated with the behavioral measure at a level of $p < 0.05$ (uncorrected) and (2) the number of adjacent nodes composing the ones that was larger than a critical cluster size, FWE corrected at $p < 0.05$ [28, 41]. Significant clusters were further examined by calculating the correlation between the relevant behavioral variable and the mean cluster-AD or mean cluster-RD. In addition, Spearman's partial correlations were performed to account for additional factors that could contribute to significance, including initial errors and asymptotic performance.

To further verify that the brain-behavior correlations in the significant cluster of nodes were not randomly generated, we applied two random sampling methods: bootstrapping and resampling. These non-parametric methods were applied while taking into account the relatively small sample size. Using bootstrapping, we resampled the mean values (mean FA or mean MD) in the significant cluster 1000 times and calculated the standard error (SE) of the distribution of correlation coefficients with the behavioral parameter. In the shuffling analysis, we randomly shuffled the behavioral data 1000 times across all participants, while the diffusivity parameters were fixed. After each shuffle, we recalculated Spearman's correlation between the shuffled behavioral measure and the diffusion parameter and created a distribution of the correlations calculated over the 1000 shuffles. Then, we calculated the likelihood ($p_{(shuffle)}$) of the original correlation value under this random distribution of correlations.

Laterality Index

Laterality indices (LIs) were calculated for each tract of each participant, in order to assess tract properties in the context of the contralateral tract. LI was calculated as the normalized difference between diffusivity properties of the left and right homologs of each tract, using the following standard formula (see [42] for a similar approach):

$$Ll = \frac{(left - right)}{(left + right)}$$

Thus, positive LIs indicate left lateralization while negative LIs indicate right lateralization. LIs were calculated over different tract parameters: mean tract-FA, the total number of streamlines, and the volume of each tract (3 LIs for each tract for each participant) [42]. Tract volume was defined as the number of voxels occupied by all streamlines for a particular fiber tract, divided by the volume of the whole-brain fiber group.

To assess the significance and direction of hemispheric lateralization for each tract, we used the non-parametric Wilcoxon signed-rank test (alpha = 0.05) under the null hypothesis that medians are equal to zero. Spearman's correlation was calculated between the degree of lateralization and the behavioral components of locomotor adaptation.

Results

Tract Identification

The ICP, SCP, and CST were successfully identified in all participants ($N = 17$). The identified tracts of interest matched previously published results, both in terms of the position of the tracts, their general shape, and the quantitative diffusivity values estimated along each tract (see Fig. 2 and Fig. S1 and compare with Figs. 3, 4, and 5 in [43] and Fig. 2 in [28]).

Brain-Behavior Correlations

To estimate the association between behavioral measures of locomotor adaptation and white matter properties, we first calculated Spearman's rank-order correlations between each behavioral measure and its corresponding mean tract
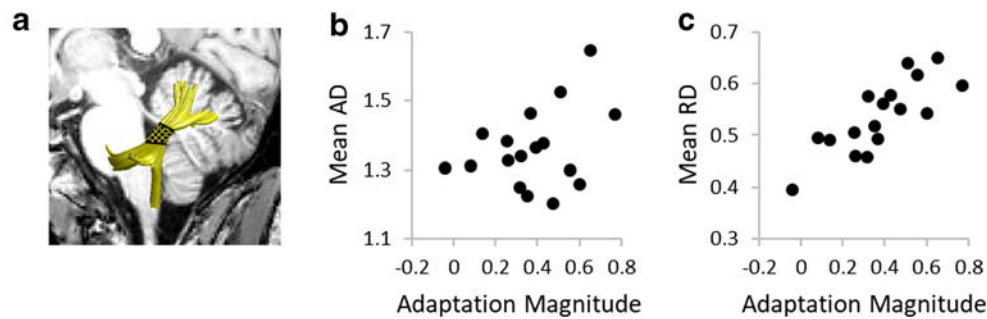
Fig. 5 The correlations in the ICP are explained by radial diffusivity (RD). **a** The left ICP is shown in a single participant, overlaid on a midsagittal T1 image of the same individual. The location of the significant cluster of nodes is indicated by a textured overlay. **b** No significant correlation was found between adaptation magnitude and the mean AD values extracted from nodes 11–16 of the left ICP ($r^2 = 0.04$, $p = 0.4321$). **c** A significant correlation was found between adaptation magnitude and the mean RD values extracted from nodes 11–16 of the left ICP ($r^2 = 0.66$, $p < 10^{-4}$)

diffusivity parameter (tract-FA or tract-MD). Mean tract-FA and mean tract-MD were calculated across all nodes, for each tract and for each individual. These analyses did not detect any significant correlation in the examined tract-behavior pairs (i.e., left ICP and adaptation magnitude, left SCP and relearning, right CST and recall, $p > 0.1$).

Averaging diffusivity along the tract is prone to wipe out the microstructural variability across the trajectory of the tract. Estimating diffusion profiles provides enhanced sensitivity for detecting localized brain-behavior correlations. Thus, we examined the associations between the relevant behavioral measures and local diffusivity values along the tract (see Methods). In accordance with our hypothesis, a significant correlation ($p < 0.05$, FWE corrected) was found between adaptation magnitude and diffusivity in the left ICP (see Fig. 3). For FA, a significant correlation ($p < 0.05$, FWE corrected) was detected in nodes 11–16 ($r = -0.58 \pm 0.12$, $\pm$ SE values derived using a bootstrap analysis, see Methods). For MD, a significant correlation ($p < 0.05$, FWE corrected) was detected in nodes 10–16 ($r = 0.69 \pm 0.11$). We further verified that these correlations were unlikely to be generated randomly, using a non-parametric shuffling analysis. Indeed, we found that the likelihood of achieving these correlation values under a random distribution (driven from the data via 1000 shuffles) was $p_{(shuffle)} = 0.013$ for FA and $p_{(shuffle)} = 0.001$ for MD.

To verify the specificity of the correlation between adaptation magnitude and diffusivity in left ICP, we repeated this analysis in the other two pathways, assessing the correlation of adaptation magnitude with diffusivity in the left SCP and in the right CST. These correlations were non-significant (see Fig. S2). In contrast with our hypotheses, however, the correlations between the right CST and recall and between the left SCP and relearning were non-significant (Fig. 4).

To further examine the microstructural factors underlying the association between the left ICP and adaptation magnitude, we calculated the mean-AD and mean-RD values within the cluster of nodes that showed significant correlations with adaptation magnitude (i.e., nodes 11:16, where both FA and

MD correlated significantly with adaptation magnitude). A significant positive correlation was found between that cluster's mean-RD and adaptation magnitude ($r = 0.81$, $p < 0.0001$). In contrast, the correlation between adaptation magnitude and the mean-AD in this cluster was non-significant ($r = 0.20$, $p = 0.43$) (Fig. 5).

To account for additional factors that could contribute to significance, we calculated Spearman's partial correlations between adaptation magnitude and diffusivity values within the significant cluster of nodes while controlling for the effects of initial errors and asymptotic performance. While the correlation between MD in the left ICP and adaptation magnitude remains significant when we partial out the effect of asymptotic performance, the other three partial correlations were non-significant (see Table S1). This is likely due to the fact that adaptation magnitude covaried with both the initial and the asymptotic asymmetry (Fig. S3), such that subjects with higher adaptation magnitude had larger asymmetry at the initial phase of adaptation and smaller asymmetry at the end of adaptation.

Lateralization Analysis

Since locomotor adaptation involves a change in the gait cycle in order to improve the symmetry between the left and right strides, we expect pathways in both the left and the right hemispheres to contribute to the adaptation process. Therefore, we expected that hemispheric asymmetry will be associated with behavioral measures of locomotor adaptation. We tested the degree of lateralization by using Wilcoxon signed-rank test under the null hypothesis that the examined tracts are not lateralized [44]. Indeed, no significant lateralization was detected in any of the examined tracts (Table S2). Next, we assessed the association between the degree of lateralization in each tract and its corresponding behavioral measure, using Spearman's correlations. This analysis revealed a significant correlation between adaptation magnitude and the individual degree of FA-lateralization in the ICP ($r = -0.78$,

$p < 0.001$; FDR corrected for 3 comparisons) (Fig. 6). Specifically, individuals who showed rightward lateralization of the ICP demonstrated higher magnitude of adaptation during the split-belt walking. Individual lateralization in the SCP and the CST was not significantly correlated with relearning and recall, respectively.

Discussion

The aim of the current study was to assess the interactions between the structural properties of the motor system and behavioral components of locomotor adaptation. Correlations were found between the magnitude of adaptation and microstructural properties of the left ICP—one of the major afferent cerebellar pathways. Specifically, we found that greater adaptation magnitude is associated with higher MD and lower FA in the left ICP. These correlations are tract-specific: they were not present in other examined tracts. Post hoc analysis revealed that these correlations are driven by radial, not axial, diffusivity. Adaptation magnitude was further associated with the degree of lateralization in the ICP, such that participants with rightward lateralization of the ICP showed higher adaptation magnitude. Additionally, no significant correlations were found between our long-term measures of locomotor learning (i.e., recall and relearning) and the predefined tracts of interest.

The cerebellum has long been known as an important structure for motor adaptation in general, and for adaptation of walking in particular [9, 18, 45, 46]. Previous studies in the visuomotor domain have implicated cerebellar white matter in the process of adaptation. For example, a tract-based spatial statistics (TBSS) analysis in healthy subjects has shown that the rate of adaptation during a visuomotor rotation task is associated with microstructural properties of cerebellar white matter [47]. Furthermore, lesions to the ICP have been associated with impaired learning during prism adaptation [6]. Our findings, linking the microstructural properties of the ICP with

the magnitude of adaptation, are consistent with these studies, and further highlight the importance of the ICP in locomotor adaptation.

The involvement of the ICP in motor adaptation can be interpreted in terms of error encoding. The ICP comprises olivo-cerebellar fibers that communicate signals from the inferior olive into the cerebellar cortex. These neuronal projections, also known as climbing fibers, form strong excitatory synapses on Purkinje cells, which in turn elicit complex spike responses. Complex spike discharge has been previously shown to encode movement errors (for review, see [48]). With respect to walking behavior, complex spike discharge has been shown to increase with perturbations applied during locomotion in the cat [21, 49, 50]. These signals have been suggested to provide a teaching signal which is capable of modifying future cerebellar activity in order to correct motor behaviors [25, 51]. In line with this view, our findings support the role of the olivo-cerebellar fibers in transmitting error signals during locomotor adaptation and suggest that the variability in the magnitude of adaptation is affected by the strength of the error signal that the Purkinje cells receive.

To account for the contribution of additional factors to the correlation between the left ICP and adaptation magnitude, such as the initial errors and asymptotic performance, we calculated Spearman's partial correlations within the significant clusters. We found that the correlation between MD in the left ICP and adaptation magnitude remains significant when we partial out the effect of asymptotic performance, but not when we partial out the effect of the initial error (Table S1). Partial correlations with FA in the left ICP were both non-significant. Thus, it is possible that the correlation with adaptation magnitude in the left ICP may be explained by variability in the initial error. Indeed, adaptation magnitude and initial errors are highly correlated (Fig. S3). This correlation, however, does not necessarily indicate that participants with large adaptation magnitude are more perturbed by the treadmill. Alternatively, we suggest that the perturbation may have affected all participants in a similar way, and the variability observed within the
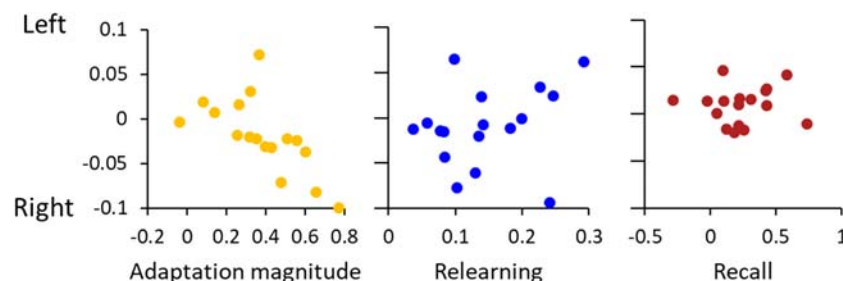
Fig. 6 Adaptation magnitude is associated with ICP lateralization. Individual lateralization of tract-FA values in the ICP (yellow), SCP (blue), and CST (red) is plotted against the participants behavioral scores on adaptation magnitude, relearning, and recall, respectively. A significant negative Spearman's correlation was found between adaptation magnitude and individual degree of FA-lateralization ($r^2 = 0.61$, $p < 0.001$;

FDR corrected), such that individuals who showed increased rightward lateralization of the ICP also demonstrated higher magnitude of adaptation. No significant correlations were found between the degree of lateralization in the SCP and relearning ($r^2 = 0.09$, $p > 0.2$), or the degree of lateralization in the CST and recall ($r^2 = 0.01$, $p > 0.6$)

initial errors may reflect an early adaptation process that occurs within the first two gait cycles.

To demonstrate this effect, we measured the association between our estimates of the first reaction to the perturbation and our measure of initial error. The first reaction to the perturbation was defined as the center-of-pressure (COP) position where the subject lifted his right (unperturbed) leg for the first time after the onset of the perturbation. This event is the first point where the reaction to the perturbation could be measured. Indeed, the position of this event changed significantly following perturbation onset (non-parametric Wilcoxon signed-rank test revealed a significant difference ($p < 0.005$) between the "first reaction" event and the comparable event in the baseline epoch).

To estimate the association between the "first reaction" to the perturbation and initial error, we calculated Spearman's correlation. This correlation was non-significant ($r = 0.39$, $p = 0.11$) (Fig. S5A). This finding suggests that the initial error may not, in fact, reflect the first reaction to the perturbation. Furthermore, to rule out the possibility that adaptation occurs already at "first reaction", we calculated a second correlation between the initial error and the difference between "first reaction" and the comparable baseline event. This correlation was also non-significant ($r = 0.0662$, $p = 0.8021$) (Fig. S5B). Taken together, these analyses suggest that the variable we term initial error does not reflect the first reaction to the perturbation or a differential effect of the perturbation on the subjects, but rather, an early phase of adaptation.

Importantly, if initial error reflects an early adaptation process, then our measure of adaptation magnitude does not capture the entire process of adaptation, but rather focuses on the slow and steady adaptation process, which is typically associated with the function of the cerebellum [52, 53]. Furthermore, the negative correlation that we found between initial error and adaptation magnitude (Fig. S3) suggests that participants with low adaptation magnitude may have adapted very quickly to the perturbation and that adaptation magnitude reflects a relative balance between the early and the late adaptation processes rather than a summarizing measure of the entire adaptation process. Future locomotion and reaching adaptation studies that include probing of the different underlying components of adaptations (slow and fast, implicit and explicit, etc.) are essential for further characterizing the adaptation processes that are associated with ICP connectivity.

The involvement of the left ICP in motor adaptation can be further interpreted in terms of its lateralization. Human motor behavior is lateralized, as can be seen in hand, leg, or eye dominance. This lateralization is usually associated with lateralization of the neural substrates (for example, see [54]). In the current study, increased rightward lateralization of the ICP was associated with increased magnitude of adaptation (Fig. 5). The rightward lateralization of the ICP may affect the reaction to the perturbation that was introduced primarily to the

left leg (typically the non-dominant leg that walked on the fast belt). To properly test this hypothesis, future studies will be necessary in which perturbation is applied to the dominant and the non-dominant legs at different phases of the experiment. Adaptation rates may then be compared as a function of dominance, and the association between the behavioral and neural asymmetry may be assessed.

Adaptation magnitude was found to be negatively correlated with FA and positively correlated with MD in the left ICP. Despite the common interpretation of FA as an index of "white matter integrity" or "connectivity strength", the relationships between the anatomical features of the tissue and FA or MD are quite complex [55]. FA is affected by various biological factors, including myelin content, axonal diameter, axonal density, directional coherence, and fiber orientation [56]. Some of these factors contribute to the efficiency of information transfer while acting to reduce FA values. For example, increased axonal diameter contributes to enhanced conduction velocity, but it is associated with decreased FA and increased RD [57–59]. Here, the negative association between FA and Adaptation Magnitude stemmed from a positive relationship with RD. This finding suggests that participants who showed a larger difference in step asymmetry have larger water mobility within the tissue in more than one direction, as in the case of enlarged axonal diameter. Because thicker axons contribute to better transfer of information, the enlarged axonal diameter may also contribute to better performance. Indeed, negative correlations between FA and task performance have been repeatedly documented in the past [30, 31, 44].

Another plausible interpretation of the negative correlation between adaptation magnitude and FA in the left ICP, and its positive correlation with MD is based on the strong negative correlation between adaptation magnitude and initial errors (Fig. S3A). As stated above, initial error may reflect an early adaptation that takes place within the first two cycles following the perturbation onset. Thus, small initial error indicates that the subjects adapted to a substantial portion of the perturbation in the first two cycles. Hence, an alternative explanation for the observed correlations is that they are driven by the early adaptation process. Indeed, we found that initial errors are negatively correlated with MD in the left ICP (Fig. S4), but the correlation with FA was non-significant. Since it has been shown that FA effects require increased statistical power in comparison to MD ([60]; see Limitations), future studies are needed to determine the association between initial errors and the ICP.

Contrary to our hypotheses, we did not find significant correlations between long-term measures of locomotor adaptation and white matter microstructure. The discrepancy between the hypotheses and the results could be explained by several factors. First, the failure to detect a significant effect in the SCP and CST may reflect limited statistical power (see

Limitations). Second, our hypotheses regarding these specific tracts were based upon functional connectivity findings previously reported in this sample [17]. It is plausible, however, that the functional connectivity between two functional regions is mediated by other brain regions, or that the variability between subjects in functional connectivity measures was transient and was not associated with structural variability.

Limitations

This study has several limitations. First, the sample size is relatively modest ($N = 17$), which reduces the statistical power of our analysis. This power was sufficient, however, to detect a significant correlation in the ICP. Furthermore, comparable sample sizes have been reported in prior published studies [30, 61–64] and have been shown to be sufficient to obtain considerable statistical power (specifically, power of 0.9 for group differences in MD, [60]). This limitation is still relevant, however, to the null effects reported here, specifically to the absence of significant correlations between long-term components of locomotor adaptation and the diffusion properties of the left SCP and the right CST. Yet, another limitation of this study concerns the scan protocol. Due to the complex behavioral and scanning protocol, which involves repeated visits in the lab to assess adaptation and relearning, and given that the focus of this study was primarily on fMRI measurements [17], the dMRI protocol was limited to a single shell measurement along 32 directions. These parameters are appropriate for tensor fitting [65] but are insufficient for fitting more complex shapes (e.g., constrained spherical deconvolution [66]). Future studies with larger sample sizes and multi-shell high angular resolution acquisition may improve sensitivity for brain-behavior correlations along the SCP and CST, and elucidate the role of these or other pathways in mediating the long-term aspects of locomotor adaptation.

Conclusions

Our study highlights the contribution of the ICP to locomotor adaptation. It delineates, for the first time, the fibers that communicate error signals to the cerebellum during locomotor adaptation in healthy human adults and supports the view that the olivo-cerebellar fibers (passing through the ICP) are important for the process of error detection during locomotor adaptation. It remains to be seen which neural mechanisms are important for the correction of these errors, and which neural pathways contribute to retaining locomotor adaptation in the long run.

Compliance with Ethical Standards

Conflict of Interest The authors declare that they have no conflict of interest.

References

1. Kawato M. Internal models for motor control and trajectory planning. Curr Opin Neurobiol. 1999;9(6):718–27.
2. Reisman DS, Block HJ, Bastian AJ. Interlimb coordination during locomotion: what can be adapted and stored? J Neurophysiol. 2005;94(4):2403–15.
3. Kluzik J, Diedrichsen J, Shadmehr R, Bastian AJ. Reach adaptation: what determines whether we learn an internal model of the tool or adapt the model of our arm? J Neurophysiol. 2008;100(3):1455–64.
4. Shadmehr R, Mussa-Ivaldi F. Adaptive representation of dynamics during learning of a motor task. J Neurosci. 1994;14(5):3208–24.
5. Bastian AJ. Understanding sensorimotor adaptation and learning for rehabilitation. Curr Opin Neurol. 2008;21(6):628–33.
6. Martin TA, Keating JG, Goodkin HP, Bastian AJ, Thach WT. Throwing while looking through prisms: I. Focal olivocerebellar lesions impair adaptation. Brain. 1996;119(4):1183–98.
7. Rabe K, Livne O, Gizewski ER, Aurich V, Beck A, Timmann D, et al. Adaptation to Visuomotor rotation and force field perturbation is correlated to different brain areas in patients with cerebellar degeneration. J Neurophysiol. 2009;101(4):1961–71.
8. Maschke M, Gomez CM, Ebner TJ, Konczak J. Hereditary cerebellar Ataxia progressively impairs force adaptation during goal-directed arm movements. J Neurophysiol. 2004;91(1):230–8.
9. Morton SM, Bastian AJ. Cerebellar contributions to Locomotor adaptations during Splitbelt treadmill walking. J Neurosci. 2006;26(36):9107–16.
10. Herzfeld DJ, Pastor D, Haith AM, Rossetti Y, Shadmehr R, O'Shea J. Contributions of the cerebellum and the motor cortex to acquisition and retention of motor memories. Neuroimage. 2014;98:147–58.
11. Galea JM, Vazquez A, Pasricha N, Orban de Xivry J-J, Celnik P. Dissociating the roles of the cerebellum and motor cortex during adaptive learning: the motor cortex retains what the cerebellum learns. Cereb Cortex. 2011;21(8):1761–70.
12. Grafton ST, Woods RP, Tyszka M. Functional imaging of procedural motor learning: relating cerebral blood flow with individual subject performance. Hum Brain Mapp. 1994;1(3):221–34.
13. Flament D, Ellermann JM, Kim S, Uğurbil K, Ebner TJ. Functional magnetic resonance imaging of cerebellar activation during the learning of a visuomotor dissociation task. Hum Brain Mapp. 1996;4(3):210–26.
14. Imamizu H, Miyauchi S, Tamada T, Sasaki Y, Takino R, Pütz B, et al. Human cerebellar activity reflecting an acquired internal model of a new tool. Nature. 2000;403(6766):192–5.
15. Shadmehr R. Neural Correlates of Motor Memory Consolidation. Science (80-). 1997;277(5327):821–5.
16. Mawase F, Haizler T, Bar-Haim S, Karniel A. Kinetic adaptation during locomotion on a split-belt treadmill. J Neurophysiol. 2013;109(8):2216–27.
17. Mawase F, Bar-Haim S, Shmuelof L. Formation of Long-term Locomotor memories is associated with functional connectivity changes in the cerebellar–thalamic–cortical network. J Neurosci. 2017;37(2):349–61.

18. Jayaram G, Tang B, Pallegadda R, Vasudevan EVL, Celnik P, Bastian A. Modulating locomotor adaptation with cerebellar stimulation. J Neurophysiol. 2012;107(11):2950–7.

19. Ito M. Error detection and representation in the olivo-cerebellar system. Front Neural Circuits. 2013;7(February):1–8.

20. Kitazawa S, Kimura T, Yin P-B. Cerebellar complex spikes encode both destinations and errors in arm movements. Nature. 1998;392(6675):494–7.

21. Andersson BYG, Armstrong DM. Complex spikes in Purkinje cells in the lateral vermis (b zone) of the cat cerebellum during locomotion. J Physiol. 1987;385(1):107–34.

22. Perrini P, Tiezzi G, Castagna M, Vannozzi R. Three-dimensional microsurgical anatomy of cerebellar peduncles. Neurosurg Rev. 2013;36(2):215–25.

23. Catani M. Thiebaut de Schotten. M. a diffusion tensor imaging tractography atlas for virtual in vivo dissections. Cortex. 2008;44(8):1105–32.

24. van Melick N, Meddeler BM, Hoogeboom TJ. Nijhuis-van der Sanden MWG, van Cingel REH. How to determine leg dominance: The agreement between self-reported and observed performance in healthy adults. Macaluso A, editor. PLoS One. 2017;12(12): e0189876.

25. Doya K. What are the computations of the cerebellum, the basal ganglia and the cerebral cortex? Neural Netw. 1999;12(7–8):961–74.

26. Leech KA, Day KA, Roemmich RT, Bastian AJ. Movement and perception recalibrate differently across multiple days of locomotor learning. J Neurophysiol. 2018;120(4):2130–7.

27. Day KA, Leech KA, Roemmich RT, Bastian AJ. Accelerating locomotor savings in learning: compressing four training days to one. J Neurophysiol. 2018;119(6):2100–13.

28. Yeatman JD, Dougherty RF, Myall NJ, Wandell BA, Feldman HM. Tract Profiles of White Matter Properties: Automating Fiber-Tract Quantification. Beaulieu C, editor. PLoS One. 2012;7(11):e49790.

29. Kronfeld-Duenias V, Amir O, Ezrati-Vinacour R, Civier O, Ben-Shachar M. The frontal aslant tract underlies speech fluency in persistent developmental stuttering. Brain Struct Funct. 2016;221(1):365–81.

30. Blecher T, Tal I, Ben-Shachar M. White matter microstructural properties correlate with sensorimotor synchronization abilities. Neuroimage. 2016;138:1–12.

31. Yablonski M, Rastle K, Taylor JSH, Ben-Shachar M. Structural properties of the ventral reading pathways are associated with morphological processing in adult English readers. Cortex. 2018:1–18.

32. Rohde GK, Barnett AS, Basser PJ, Marenco S, Pierpaoli C. Comprehensive approach for correction of motion and distortion in diffusion-weighted MRI. Magn Reson Med. 2004;51(1):103–14.

33. Friston KJ, Ashburner J. Generative and recognition models for neuroanatomy. Neuroimage. 2004;23(1):21–4.

34. Leemans A, Jones DK. The B -matrix must be rotated when correcting for subject motion in DTI data. Magn Reson Med. 2009;61(6):1336–49.

35. Roemmich RT, Long AW, Bastian AJ. Seeing the errors you feel enhances Locomotor performance but not learning. Curr Biol. 2016;26(20):2707–16.

36. Reisman DS, Wityk R, Silver K, Bastian AJ. Locomotor adaptation on a split-belt treadmill can improve walking symmetry post-stroke. Brain. 2007;130(7):1861–72.

37. Basser PJ, Pajevic S, Pierpaoli C, Duda J, Aldroubi A. In vivo fiber tractography using DT-MRI data. Magn Reson Med. 2000;44(4):625–32.

38. Mori S, Crain BJ, Chacko VP, Van Zijl PCM. Three-dimensional tracking of axonal projections in the brain by magnetic resonance imaging. Ann Neurol. 1999;45(2):265–9.

39. Bruckert L, Shpanskaya K, McKenna ES, Borchers LR, Yablonski M, Blecher T, et al. Age-dependent white matter characteristics of the cerebellar peduncles from infancy through adolescence. Cerebellum. 2019;18(3):372–87.

40. Wakana S, Caprihan A, Panzenboeck MM, Fallon JH, Perry M, Gollub RL, et al. Reproducibility of quantitative tractography methods applied to cerebral white matter. Neuroimage. 2007;36(3):630–44.

41. Nichols TE, Holmes AP. Nonparametric permutation tests for functional neuroimaging: a primer with examples. Hum Brain Mapp. 2002;15(1):1–25.

42. Thiebaut de Schotten M, Ffytche DH, Bizzi A, Dell'Acqua F, Allin M, Walshe M, et al. Atlasing location, asymmetry and inter-subject variability of white matter tracts in the human brain with MR diffusion tractography. Neuroimage. 2011;54(1):49–59.

43. Leitner Y, Travis KE, Ben-Shachar M, Yeom KW, Feldman HM. Tract profiles of the cerebellar white matter pathways in children and adolescents. Cerebellum. 2015;14(6):613–23.

44. Travis KE, Leitner Y, Feldman HM, Ben-Shachar M. Cerebellar white matter pathways are associated with reading skills in children and adolescents. Hum Brain Mapp. 2015;36(4):1536–53.

45. Bastian AJ. Learning to predict the future: the cerebellum adapts feedforward movement control. Curr Opin Neurobiol. 2006;16(6):645–9.

46. Statton MA, Vazquez A, Morton SM, Vasudevan EVL, Bastian AJ. Making Sense of Cerebellar Contributions to Perceptual and Motor Adaptation 2018;111–121.

47. Della-Maggiore V, Scholz J, Johansen-Berg H, Paus T. The rate of visuomotor adaptation correlates with cerebellar white-matter microstructure. Hum Brain Mapp. 2009;30(12):4048–53.

48. Streng ML, Popa LS, Ebner TJ. Complex spike wars: a new Hope. Cerebellum. 2018;17(6):735–46.

49. Kim JH, Wang JJ, Ebner TJ. Climbing fiber afferent modulation during treadmill locomotion in the cat. J Neurophysiol. 1987;57(3):787–802.

50. Lou JS, Bloedel JR. Responses of sagittally aligned Purkinje cells during perturbed locomotion: relation of climbing fiber activation to simple spike modulation. J Neurophysiol. 1992;68(5):1820–33.

51. Herzfeld DJ, Kojima Y, Soetedjo R, Shadmehr R. Encoding of error and learning to correct that error by the Purkinje cells of the cerebellum. Nat Neurosci. 2018;21(5):736–43.

52. McDougle SD, Bond KM, Taylor JA. Explicit and implicit processes constitute the fast and slow processes of sensorimotor learning. J Neurosci. 2015;35(26):9568–79.

53. Butcher PA, Ivry RB, Kuo SH, Rydz D, Krakauer JW, Taylor JA. The cerebellum does more than sensory prediction error-based learning in sensorimotor adaptation tasks. J Neurophysiol. 2017;118(3):1622–36.

54. Büchel C, Raedler T, Sommer M, Sach M, Weiller C, Koch MA. White matter asymmetry in the human brain: a diffusion tensor MRI study. Cereb Cortex. 2004;14(9):945–51.

55. Jones DK, Knösche TR, Turner R. White matter integrity, fiber count, and other fallacies: the do's and don'ts of diffusion MRI. Neuroimage. 2013;73:239–54.

56. Beaulieu C. The basis of anisotropic water diffusion in the nervous system - a technical review. NMR Biomed. 2002;15(7–8):435–55.

57. Barazany D, Basser PJ, Assaf Y. In vivo measurement of axon diameter distribution in the corpus callosum of rat brain. Brain. 2009;132(5):1210–20.

58. Horowitz A, Barazany D, Tavor I, Bernstein M, Yovel G, Assaf Y. In vivo correlation between axon diameter and conduction velocity in the human brain. Brain Struct Funct. 2015;220(3):1777–88.

59. Lee DL, Strathmann FG, Gelein R, Walton J, Mayer-Proschel M. Iron deficiency disrupts axon maturation of the developing auditory nerve. J Neurosci. 2012;32(14):5010–5.

60. De Santis S, Drakesmith M, Bells S, Assaf Y, Jones DK. Why diffusion tensor MRI does well only some of the time: variance

and covariance of white matter tissue microstructure attributes in the living human brain. Neuroimage. 2014;89:35–44.

61. Kronfeld-Duenias V, Civier O, Amir O, Ezrati-Vinacour R, Ben-Shachar M. White matter pathways in persistent developmental stuttering: lessons from tractography. J Fluen Disord. 2018;55:68–83.

62. Schlegel AA, Rudelson JJ, Tse PU. White Matter Structure Changes as Adults Learn a Second Language; 2012. p. 1664–70.

63. Gomez J, Pestilli F, Yoon J, Grill-spector K, Gomez J, Pestilli F, et al. Functionally defined white matter reveals segregated pathways in human ventral temporal cortex associated with category-specific functionally defined white matter reveals segregated pathways in human ventral temporal cortex associated with category-Specif. Neuron. 2015;85(1):216–27.

64. Klingberg T, Hedehus M, Temple E, Salz T, Gabrieli JDE, Moseley ME, et al. Microstructure of Temporo-Parietal White Matter as a Basis for Reading Ability : Evidence from Diffusion Tensor Magnetic Resonance Imaging. 2000;25:493–500.

65. Rokem A, Yeatman JD, Pestilli F, Kay KN, Mezer A, Walt S Van Der, et al. Evaluating the Accuracy of Diffusion MRI Models in White Matter 2015;1–26.

66. Tournier JD, Yeh CH, Calamante F, Cho KH, Connelly A, Lin CP. Resolving crossing fibres using constrained spherical deconvolution: validation using diffusion-weighted imaging phantom data. Neuroimage. 2008;42(2):617–25.